a 702-keV $M1$ transition to the 152-keV state and a 384-keV $E1$ transition, of comparable intensity, to the 472-keV level. The $\frac{5}{2}$ spin observed in the correlation measurements for a state near 850 keV might well belong to the 846-keV state.

The 473-, 1178, and 1810-keV levels were all reached by strong p-wave transitions in stripping measurements[4] and therefore should have spin $\frac{1}{2}^-$ or $\frac{3}{2}^-$. It was noted above that the 473-keV state most likely has spin $\frac{3}{2}^-$. Since it is found that the 1810-keV state decays to both the ground state $(\frac{7}{2}^-)$ and 1178-keV states with comparable intensities, it is suggested that the 1810-keV state also, most likely, has spin $\frac{3}{2}^-$ rather than $\frac{1}{2}^-$. The decay of the 1178-keV level shows no observable branch to the ground state. This is in striking contrast to the behavior of the 473- and 1810-keV levels which show strong ground-state transitions. This may be an indication that the 1178-keV level has spin and parity $\frac{1}{2}^-$, although this question cannot be settled on the basis of the present measurements.

ACKNOWLEDGMENTS

The authors are indebted to Harry Mann at Argonne National Laboratory for the use of the Ge(Li) detector and to Professor H. E. Gove and Professor D. Cline for numerous helpful discussions.

PHYSICAL REVIEW VOLUME 155, NUMBER 4 20 MARCH 1967

Elastic Scattering of He^3 Ions at Intermediate Energies*

E. F. GIBSON,† B. W. RIDLEY,‡ J. J. KRAUSHAAR, AND M. E. RICKEY§
Department of Physics and Astrophysics, University of Colorado, Boulder, Colorado
AND
R. H. BASSEL||
Oak Ridge National Laboratory, Oak Ridge, Tennessee
(Received 24 October 1966)

The elastic scattering of He^3 ions has been studied at 37.7 MeV from Ca^{40}, Fe^{56}, and Ni^{58} and at 43.7 MeV from Ni^{58}, Y^{89}, and Zr^{90}. A theoretical analysis has been carried out in terms of the optical model. Both discrete and continuous ambiguities in the optical-model parameters appear, and are discussed in some detail. An average potential has been selected which adequately accounts for our data as well as some reaction data of others. In the case of Ca^{40} and Ni^{58}, the energy dependence of the real and imaginary well depths has been investigated using a standard geometry. Similarly, the A dependence of the well depths has been examined.

I. INTRODUCTION

THE validity of an optical-model description of the scattering of complex particles by nuclei has been clearly demonstrated in extensive studies of the elastic scattering of deuterons and α particles over a wide energy range. In contrast with nucleon scattering, many parameter sets have been found to give equally good representations of the data, showing ambiguities of a both discrete and continuous nature.[1–3] Nevertheless, systematic trends with bombarding energy and nuclear composition have been discerned,[1] consistent with the concept of "gross properties" inherent in the optical model.

Theoretical treatments of the optical potential for complex incident particles predict a real potential-well depth approximately equal to the optical potential for one nucleon multiplied by the number of nucleons in the incident particle.[4] This potential may be modified substantially by changes in binding energy of the particle when it enters the nucleus,[5] leading to a dependence on incident energy that differs from that for nucleon scattering. While optical analyses of elastic scattering have failed to determine a unique potential, it appears that particle transfer reactions may be more sensitive to conditions in the nuclear interior, and such evidence as there is provides qualitative support for these theoretical expectations.[6–9]

The demonstrable value of systematic studies as a

* Research sponsored by the U. S. Atomic Energy Commission under contract with the Union Carbide Corporation and the University of Colorado.
† Present address: University of Oregon, Eugene, Oregon.
‡ Permanent address: Atomic Energy Research Establishment, Harwell, England.
§ Present address: University of Indiana, Bloomington, Indiana.
|| Present address: Brookhaven National Laboratory, Upton, New York.
[1] C. M. Perey and F. G. Perey, Phys. Rev. **132**, 755 (1963).
[2] L. McFadden and G. R. Satchler, Nucl. Phys. **84**, 177 (1966).
[3] C. R. Bingham, M. L. Halbert, and R. H. Bassel, Phys. Rev. **148**, 1174 (1966).
[4] M. A. Melkanoff, T. Sawada, and N. Cindro, Phys. Rev. Letters **2**, 98 (1962); J. R. Rook, Nucl. Phys. **61**, 219 (1965).
[5] H. W. Wittern, Nucl. Phys. **62**, 628 (1965).
[6] R. M. Drisko and F. Rybicki, Phys. Rev. Letters **16**, 275 (1966).
[7] D. Cline, W. P. Alford, and L. M. Blau, Nucl. Phys. **73**, 33 (1965).
[8] M. M. Stautberg and J. J. Kraushaar, Phys. Rev. **151**, 969 (1966).
[9] R. H. Bassel, R. M. Drisko, G. R. Satchler, L. L. Lee, J. P. Schiffer, and B. Zeidman, Phys. Rev. **136**, B160 (1964).

function of bombarding energy and target nucleus composition suggests that studies with other incident particles would further our understanding of the nature of the optical potential for complex particles. He^3 scattering may be expected to show many features in common with the strongly absorbed α particle, while its different binding energy and radius may prove useful in checking such a model as that proposed by Wittern.[5] Furthermore, the spin of $\frac{1}{2}$ adds the variety of polarization phenomena.

For such studies, analyses of energy dependence are of importance. He^3 elastic scattering has been reported at energies of 8.5 and 9.5 MeV,[7] 12 MeV,[10] 20 MeV,[11] 22 MeV,[12] 30 MeV,[13] and 33 MeV.[14] Springer *et al.*[15] have compared He^3 and α-particle scattering by Ca^{40} at equal momenta, where the He^3 energy was 64.3 MeV. Optical-model analyses of these data suggest that there are ambiguities in parameters similar to those observed for other strongly absorbed particles. Parameter sets have been found with real potential-well depths in the range 6 to 45 MeV,[16–18] and others with values near to 60 MeV,[11,13] 95 MeV,[10,11] 130 MeV,[12,14] and 170 MeV.[7,12] These are reminiscent of the discrete ambiguities separated by steps of 30 to 40 MeV in real potential observed in analyses of deuteron[1,19,20] and α-particle scattering.[2,21]

The work reported in this paper extends He^3 scattering data for medium-weight nuclei to the higher energies of 37.7 and 43.7 MeV, with the intention of furthering systematic studies of energy and mass dependence, and to provide optical parameters needed for distorted-wave analyses of He^3 inelastic scattering and (He^3,d) and (He^3,α) reactions. Data for He^3 inelastic scattering and reactions were obtained at the same time as those on elastic scattering, and the results from the inelastic scattering will be presented in the following paper. A detailed study of parameter ambiguities has been made in the case of Ni^{58} and evidence from He^3 reactions which may limit these will be discussed. A study of energy dependence of the real and imaginary well depths for Ca^{40} and Ni^{58} has also been made, using a fixed geometry that represents an average of geometries that best fit data on different targets at 37.7 MeV. In this latter study, use has been made of all available data on scattering by these nuclei. A more detailed account of the measurements reported here and numerical values of the cross sections are included in Ref. 21a.

II. EXPERIMENTAL APPARATUS

The He^3 ions were accelerated with the University of Colorado variable energy cyclotron to energies of 37.7 and 43.7 MeV. Beam currents in the scattering chamber ranged up to 800 μA. An He^3 recovery system was used that is similar to one described by Wegner and Hall.[22]

The deflected beam from the cyclotron passed through the beam handling system shown in Fig. 1. Dispersion in the cyclotron fringe field facilitated momentum analysis by slits placed at the intermediate image, with a horizontal spacing ranging from 0.015 to 0.060 in. Collimators in the scattering chamber limited the beam spot size on the target to approximately $\frac{1}{16}$-in. diameter for runs at small scattering angles and approximately $\frac{1}{8}$-in. diameter for runs at larger angles.

The unscattered beam collected in a Faraday cup was measured with a current to frequency conversion system[23] that fed pulses, each representing a given collected charge, into the first channel of a ND-160 pulse-height analyzer. The accuracy of this system is limited at small currents by a zero instability of the order of 0.1 nA.

The 36-in. scattering chamber (see Fig. 1) contains a five-position target mount and two detector trays that rotate independently in the scattering plane. The angular positions of the detectors were remotely controlled with a precision of 0.1°.

The scattered particles were detected in a telescope of two Ortec[24] transmission-type silicon surface barrier detectors 50 mm^2 in area, biased for total depletion and cooled to dry-ice temperature. The first detector was either 200 or 388 μ thick and the second either 1090 or 2000 μ thick. The combination was such that all He^3 particles were stopped. For most of the runs a defining aperture $\frac{1}{8}$-in. diameter placed immediately in front of the first detector limited the angular resolution in the scattering plane to 1.4° when the distance from the target was 7 in. For runs at small angles, a slit 0.058 in. wide at 14 in. from the target was used to give an angular resolution less than 0.4°.

Overlapping energy spectra of scattered He^3 and other reaction products were separated with the aid of

[10] J. L. Yntema, B. Zeidman, and R. H. Bassel, Phys. Letters **11**, 302 (1964).
[11] R. W. Klingensmith, H. J. Hausman, and W. D. Ploughe, Phys. Rev. **134**, B1220 (1964).
[12] D. D. Armstrong, A. C. Blair, and R. H. Bassel (private communication).
[13] G. W. Greenlees, J. S. Lilley, P. C. Rowe, and P. E. Hodgson, Nucl. Phys. **24**, 334 (1961).
[14] R. H. Siemssen, T. H. Braid, D. Dehnhard, and B. Zeidman, Phys. Letters **18**, 155 (1965).
[15] A. Springer, M. Chabre, D. L. Hendrie, and H. G. Pugh, Phys. Letters **20**, 397 (1966).
[16] P. E. Hodgson, Nucl. Phys. **21**, 28 (1960).
[17] J. A. Aguilar, W. E. Burcham, J. B. A. England, A. Garcia, P. E. Hodgson, P. V. March, J. S. C. McKee, E. M. Mosinger, and W. T. Toner, Proc. Roy. Soc. (London) **A257**, 13 (1960).
[18] J. A. Aguilar, J. B. A. England, P. E. Hodgson, and W. T. Toner, Nucl. Phys. **25**, 259 (1961).
[19] R. M. Drisko, G. R. Satchler, and R. H. Bassel, Phys. Letters **5**, 347 (1963).
[20] H. R. E. Tjin, A. Djie, and K. W. Brockman, Jr., Nucl. Phys. **74**, 417 (1965).
[21] H. W. Broek, J. L. Yntema, B. Buck, and G. R. Satchler, Nucl. Phys. **64**, 259 (1965).
[21a] E. F. Gibson, thesis, University of Colorado, 1966 (unpublished).
[22] H. E. Wegner and W. S. Hall, Rev. Sci. Instr. **29**, 1100 (1958).
[23] P. W. Allison, Rev. Sci. Instr. **35**, 1728 (1964).
[24] Oak Ridge Technical Enterprises Corporation, Oak Ridge, Tennessee.

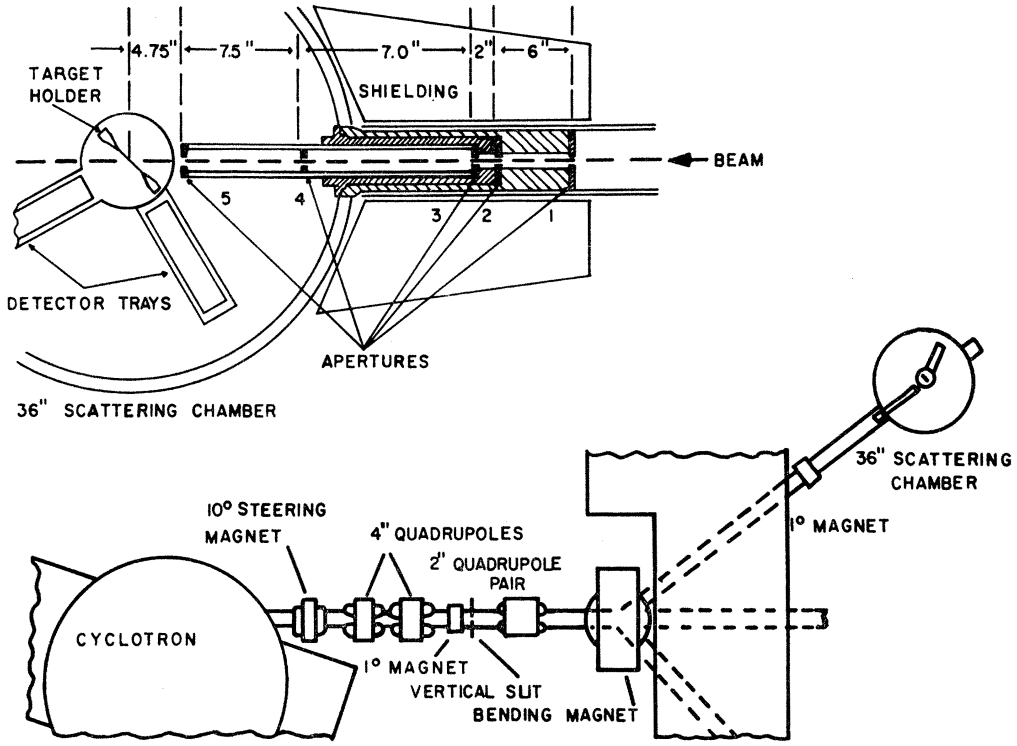

FIG. 1. Experimental arrangement for the He^3 scattering measurements.

an $(E,\Delta E)$ particle identification system. Pulses from the front detector (ΔE) and the rear detector (E') were amplified and fed into a multiplier circuit that gave an output signal proportional to $\Delta E(E'+K_1\Delta E+K_2)$. Using as a guide the approximate relation $E\Delta E\sim Mz^2$, where M is the mass and z the charge of the detected particle, and $E=\Delta E+E'$, K_1 and K_2 were adjusted empirically to obtain signals proportional to Mz^2 that were nearly independent of energy. The pulse multiplier used was based on a design by Radeka and Miller[25] using field-effect transistors.

Pulses proportional to total energy were obtained by adding directly the signals from the two detectors in a manner described previously.[26] This eliminates the problem of matching amplifier gains, and works satisfactorily except when the ΔE detector is so thin that capacity breakthrough of the large E' signal into the ΔE channel occurs. The summed signal, E, was amplified by a Tennelec[27] preamplifier model No. 101, and fed into the low-level input of the ND-160 pulse-height analyzer. Analyzed signals were then routed into one of four 1024-channel groups of the analyzer memory according to the nature of the detected particle as selected by discriminators viewing the output of the pulse multiplier.

The targets used in this experiment are listed in Table I. Also shown are their thicknesses and enrichments. All the targets were self-supporting foils. The Zr^{90}, Ni^{58}, and Fe^{56} were isotopically enriched metal foils obtained from Oak Ridge.[28] The Ca^{40} targets were produced by vacuum deposition of natural calcium. Self-supporting Ca^{40} targets as thin as 0.4 mg/cm^2 were produced in this manner.

The thicknesses of the Fe^{56}, Ni^{58}, and Zr^{90} targets were determined by weighing. The Ca^{40} and Y^{89} samples could not be weighed conveniently so their thicknesses were determined from the energy lost by Am^{241} α particles in passing through them. The thickness of the targets were uniform within 5%. The cyclotron beam spot did not vary appreciably in position during the course of the experiment. For each target,

TABLE I. Thicknesses and enrichments of the targets used.

Target	Thickness(mg/cm^2)	Enrichment
Ca^{40}	0.86	96.97%(nat.)
Ca^{40}	0.81	96.97%(nat.)
Fe^{56}	1.65	>99%
Ni^{58}	0.87	99.3%
Y^{89}	0.62	100%
Zr^{90}	2.39	97.8%

[25] G. L. Miller and V. Radeka, Brookhaven National Laboratory Report No. BNL-6952 (unpublished); V. Radeka, IEEE Trans. Nucl. Sci. 11, 312 (1964).
[26] R. Sherr, B. Bayman, E. Rost, M. E. Rickey, and C. Hoot, Phys. Rev. 139, B1272 (1965),
[27] Tennelec Instrument Company, Oak Ridge, Tennessee.
[28] Isotopes Sales Department, Oak Ridge National Laboratory, Oak Ridge, Tennessee.

the over-all normalization of cross sections, into which the target thickness enters, was found to agree within 5% with cross sections at small angles down to 3° calculated from the optical model. In this angular range, scattering is dominated by the Coulomb interaction and is insensitive to details of the nuclear potential provided this gives an approximate fit to large-angle cross sections. The cross sections, however, were calculated using the thicknesses of the targets and the normalization to Coulomb scattering served only as a check on the errors assigned.

III. EXPERIMENTAL PROCEDURE AND DATA ANALYSIS

The analyzer gain was adjusted so that pulses corresponding to the most energetic particles of interest fell near the highest channel available. The conversion gain under these conditions was as large as 58 keV per channel. The apparent energy resolution was appreciably worsened by the large conversion gain.

A spectrum taken with Fe^{56} is shown in Fig. 2. The energy resolution (full width at half-maximum, FWHM) is about 200 keV and the effects of the large conversion gain can be clearly seen. Although particle analysis was used, it sometimes happened that alpha groups were still counted in the He^3 spectra. One such group above the elastic peak is shown in Fig. 2, although in general, alpha contamination was far weaker than this. The main contaminant peaks in the spectra were elastic scattering peaks from O^{16} and C^{12}. Because of the lack of knowledge of the behavior of the cross sections of He^3 scattering from O^{16} and C^{12}, no corrections were made for their contributions where they had coalesced with the elastic group of interest. The maximum contribution of these two was judged to be less than 5%.

The data from the analyzer was finally converted to a linear or logarithmic plot and a listing that included

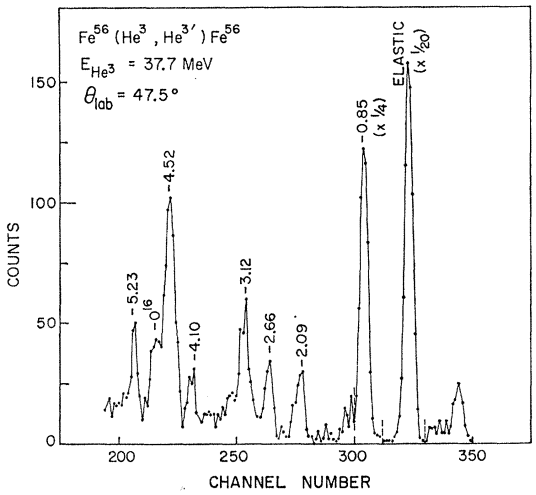

FIG. 2. An energy spectrum of 37.7-MeV He^3 ions scattered by Fe^{56}.

a running sum of the counts in each channel. Cross sections were extracted by summing the number of counts in the peak and subtracting an estimated background. No dead-time correction for the pulse-height analyzer had to be made since the pulses from the beam integration system were also stored in the analyzer.

The errors associated with differential cross sections shown in the figures are relative errors based on the statistical error on the number of counts in the peak and the background with an additional error because of the uncertainty in judging the background. Where no error bars are shown, the errors are less than the diameter of the data point. The absolute uncertainty on the cross sections is judged to be about 5%.

The angular asymmetry was determined by comparing relative elastic cross sections taken on both sides of the beam direction. The relative angular distribution obtained for measurements on the right were then compared to those on the left. These curves were shifted with respect to angle only until they coincide. The difference in angle then gave the total angular asymmetry of the system, and all detector angles were then corrected by half this value.

For measurements with scattering angles less than 15° the solid angle subtended by the detector was reduced considerably. The beam currents, however, had to be reduced to such small values that the zero drift of the beam integration system became significant. Therefore, a small monitor detector was placed at a fixed angle and the target angle was kept fixed at 0°. The ratio of the monitor counts to the integrator counts, which should be a constant, was used to correct the integrator counts. This correction was as large as 50% at 3° and usually dropped to zero at 6°.

The beam energy was determined by the cross-over method,[29] in which one finds the angle at which particles elastically scattered by one nucleus have the same energy as those inelastically scattered with a known Q value by a heavier nucleus. The choice of a suitable pair of nuclides depends upon the energy and nature of the incident beam. In this experiment the crossovers that were observed were of He^3 elastically scattered by O^{16} and inelastically scattered with Q values of -3.73 or -4.48 MeV by Ca^{40}, using an oxidized calcium target. These crossovers occur at angles near to 60° for incident energies E around 40 MeV, and $d\theta/dE$ has the value 1 deg/MeV.

Since inelastic data were taken with the Ca^{40} target, an accurate energy determination was made in that case using this method. The energy of the He^3 beam was found to be 37.7 MeV. The higher energy value, 43.7 MeV, was established by the shift in the elastic peak from Fe^{56} when data were obtained during the same run both at the low and high energy and by a knowledge of the conversion gain. Angular distributions

[29] B. M. Bardin and M. E. Rickey, Rev. Sci. Instr. **35**, 902 (1964).

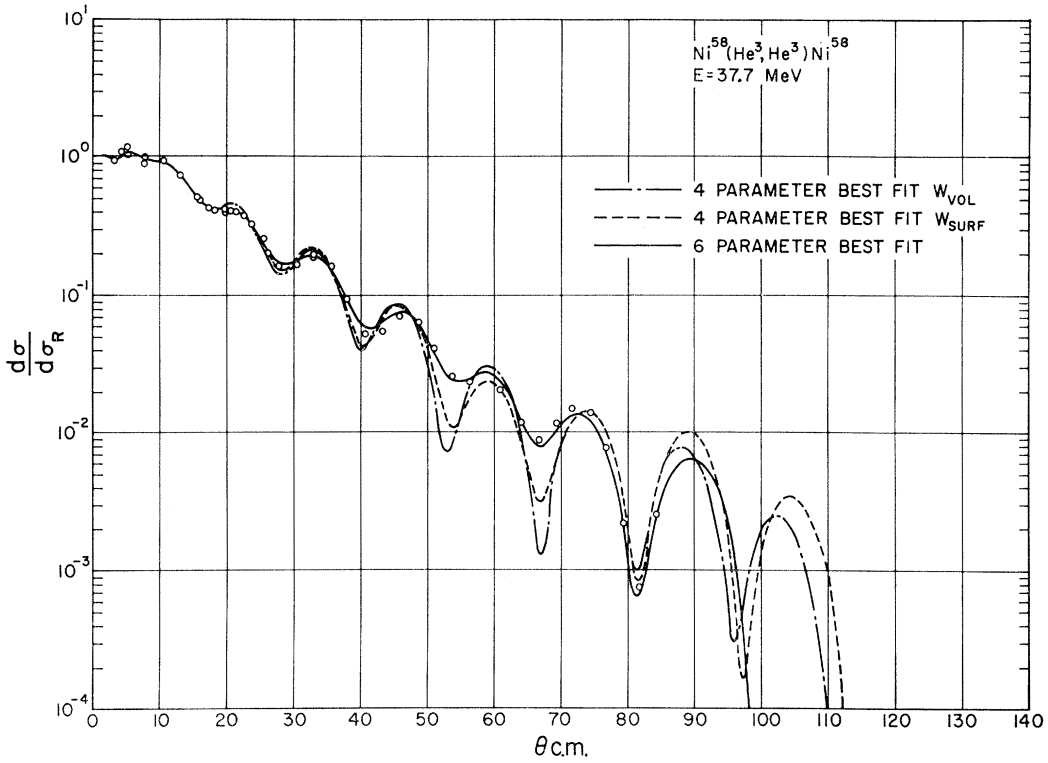

FIG. 3. Comparison of four- and six-parameter fits to the experimental angular distribution for Ni^{58} at 37.7 MeV. In the four-parameter fit labeled W_{VOL}, the imaginary potential has the same geometry as the real potential. For W_{SURF} the imaginary geometry is the radial differential of the real geometry.

were run on other targets at other times at either of these two energies. Although no direct energy measurements were made for these other runs, it appeared from a knowledge of the zero-energy channel and the conversion gain that these beam energies were reproducible to within 0.5 MeV.

IV. OPTICAL-MODEL ANALYSIS

The elastic scattering was analyzed for the most part in terms of an optical-model potential of the form

$$V(r)=-U_0(e^x+1)^{-1}-iW_0(e^{x'}+1)^{-1}+V_c,$$

where

$$x=(r-r_0A^{1/3})/a, \quad x'=(r-r_0'A^{1/3})/a'.$$

The term V_c is the Coulomb potential due to a uniformly charged sphere of charge radius $r_c=1.4A^{1/3}$ F.

Optical-model parameters were determined by fitting the data with the aid of two automatic search routines[30] which minimize the quantity

$$\chi^2=\sum_{i=1}^{N}\{[\sigma_{TH}(\theta_i)-\sigma_{EX}(\theta_i)]/\Delta\sigma(\theta_i)\}^2.$$

For all of the analysis presented in Secs. V, VII, and VIII, the experimental uncertainty $\Delta\sigma$ was set equal to 5% of σ_{EX} for each experimental point. For the optical-parameter searching that resulted in the "standard" fits discussed in Sec. VI, a slightly different weighting was used. The values at the very small angles ($<15°$) were assigned an uncertainty of 5% mainly because of the uncertainty in scattering angles. Above 15°, the statistical error from the number of counts was used which ranged from a few percent at small angles to about 5% at the larger angles. All quoted values of χ^2 were obtained using the constant 5% uncertainty.

The spin-orbit interaction was assumed to be zero, mainly for the reason that its magnitude is unknown at the present time. Also, its influence on the elastic scattering of He^3 particles is probably quite weak, as evidenced by a trial calculation with a spin-orbit interaction of the same strength as that required to fit proton scattering. In this trial, differential cross sections for scattering of 37.7-MeV He^3 ions by Ca^{40} were calculated using the standard parameters for the central potential given in Table IV, both with and without a spin-orbit potential with parameters $V_s=6$ MeV, $r_s=1.05$ F, and $a_s=0.80$ F. The effect of the spin-orbit potential in the angular range of interest was negligible below 55°. At larger angles it filled in the deep minima and decreased the maxima by some 20%.

Some parameter searches were attempted using a four-parameter optical model in which the imaginary potential either had the same geometry as the real potential, or had a form that was the radial derivative

[30] Optical-model search code written by F. G. Perey. Optical-model search code HUNTER written by R. M. Drisko.

TABLE II. Comparison of the optical-model parameters for Ni^{58} at 37.7 MeV obtained with four- and six-parameter searches.

U_0 (MeV)	r_0(F)	a(F)	W_0(MeV)	r_0'(F)	a'(F)	χ^2
170.0[a]	1.169	0.738	33.2			1179
171.8[b]	1.200	0.730	115.7			1570
172.6[c]	1.147	0.712	20.16	1.562	0.802	254

[a] Four-parameter fit with surface imaginary potential.
[b] Four-parameter fit with volume imaginary potential.
[c] Six-parameter fit with volume imaginary potential.

of the real potential. The results are summarized in Fig. 3 where the best four-parameter fits with the volume and derivative imaginary potentials are shown along with the best fit for the six-parameter case where the imaginary potential had a volume form but with parameters different from those of the real. The parameters and values of χ^2 for the three fits are given in Table II. Both four-parameter potentials predicted oscillations of amplitude far greater than those of the data. It was thus felt that six parameters were needed to provide acceptable fits, and the further analyses were conducted on this basis. In the six-parameter model that will be discussed, the choice of a volume rather than derivative form for the imaginary potential, though somewhat arbitrary, was guided by evidence that the former provides slightly better agreement with the existing data.

The inadequacy of the four-parameter model in the present instance contrasts with some recently reported studies for 12-MeV elastic triton scattering.[31] On the other hand, Broek *et al.*[21] have found that α-particle scattering at 43 MeV could not be fitted well with a four-parameter potential. Their best fits required an imaginary potential whose radius exceeded that of the real potential.

V. POTENTIAL AMBIGUITIES

Optical-model fits to He^3 scattering may be expected to evince ambiguities like those observed in studies of deuteron[1,20] and α-particle scattering.[2,21] The variety of potentials that has been found by other groups to fit He^3 data does indeed suggest that this is so. In order to explore these ambiguities, the He^3 scattering data from Ni^{58} at 37.7 MeV were used as a test case in the hope that they would furnish a representative situation for the targets and incident energies of interest in this paper.

Three groups of parameter searches were carried out in this investigation. Within one group χ^2 was minimized for each of a number of different fixed values of U_0 by varying the same set of parameters. The groups differed in the parameters that were varied. The geometrical parameters from which these searches were started had been found in preliminary investigations[32] to fit all of the 37.7- and 43.7-MeV data except Ca^{40} with minor and fairly systematic variations of well depth. These parameters and the potential depths that fit the Ni^{58} data at 37.7 MeV are included in Table IV. The searches that led to them were started from parameter sets that had been found by Armstrong, Blair, and Bassel[12] to fit He^3 scattering data for several isotopes at 22 MeV.

In group I, only r_0 and a were varied to minimize χ^2 for each value of U_0. The imaginary potential was fixed, W_0, r_0' and a' being assigned the values given in Table IV.

In group II, W_0, r_0 and a were allowed to vary. The geometry of the imaginary potential remained fixed with the previously quoted values of r_0' and a'.

The results of these searches are summarized in Fig. 4. Several discrete minima in χ^2 are evident, namely in the regions where U_0 is about 60, 120, and 180 MeV. The values of U_0 that minimize χ^2 for fixed W_0 are not changed when W_0 is allowed to vary, although this gives substantial improvement in fit in some instances. The values of r_0 and a that minimize χ^2 likewise differ by not more than a few percent between groups I and II.

The fits obtained for the different potentials that minimize χ^2 in the group-II search are shown in Fig. 5. Only at back angles do the predictions diverge substantially, and it is possible that additional data in this angular range could further limit the number of acceptable potentials. The asymptotic wave functions corresponding to these three potentials are characterized by the partial-wave reflection coefficients, η_L, shown in Table III, and are seen to be closely similar. The feature that distinguishes the different wave functions is the number of half-wavelengths within the nuclear potential of partial waves with small angular

TABLE III. The partial-wave reflection coefficients for the Ni^{58} potentials that minimize χ^2.

L	$\lvert\eta_L\rvert$, $U_0=60$	$\lvert\eta_L\rvert$, $U_0=120$	$\lvert\eta_L\rvert$, $U_0=180$
0	0.011	0.014	0.016
1	0.010	0.016	0.017
2	0.011	0.014	0.016
3	0.012	0.016	0.017
4	0.010	0.013	0.015
5	0.014	0.016	0.016
6	0.007	0.013	0.015
7	0.018	0.015	0.014
8	0.013	0.019	0.018
9	0.021	0.017	0.020
10	0.048	0.045	0.043
11	0.064	0.073	0.076
12	0.160	0.167	0.159
13	0.306	0.311	0.299
14	0.515	0.510	0.489
15	0.700	0.685	0.667
16	0.820	0.808	0.794
17	0.893	0.884	0.876
18	0.936	0.931	0.926
19	0.963	0.959	0.956
20	0.979	0.977	0.975
21	0.989	0.988	0.987
22	0.999	0.994	0.994
23	0.998	0.997	0.997
24	0.999	0.999	0.999

[31] R. N. Glover and A. D. W. Jones, Nucl. Phys. **81**, 268 (1966).
[32] E. F. Gibson, J. J. Kraushaar, M. E. Rickey, B. W. Ridley, and R. H. Bassel, Bull. Am. Phys. Soc. **11**, 118 (1966).

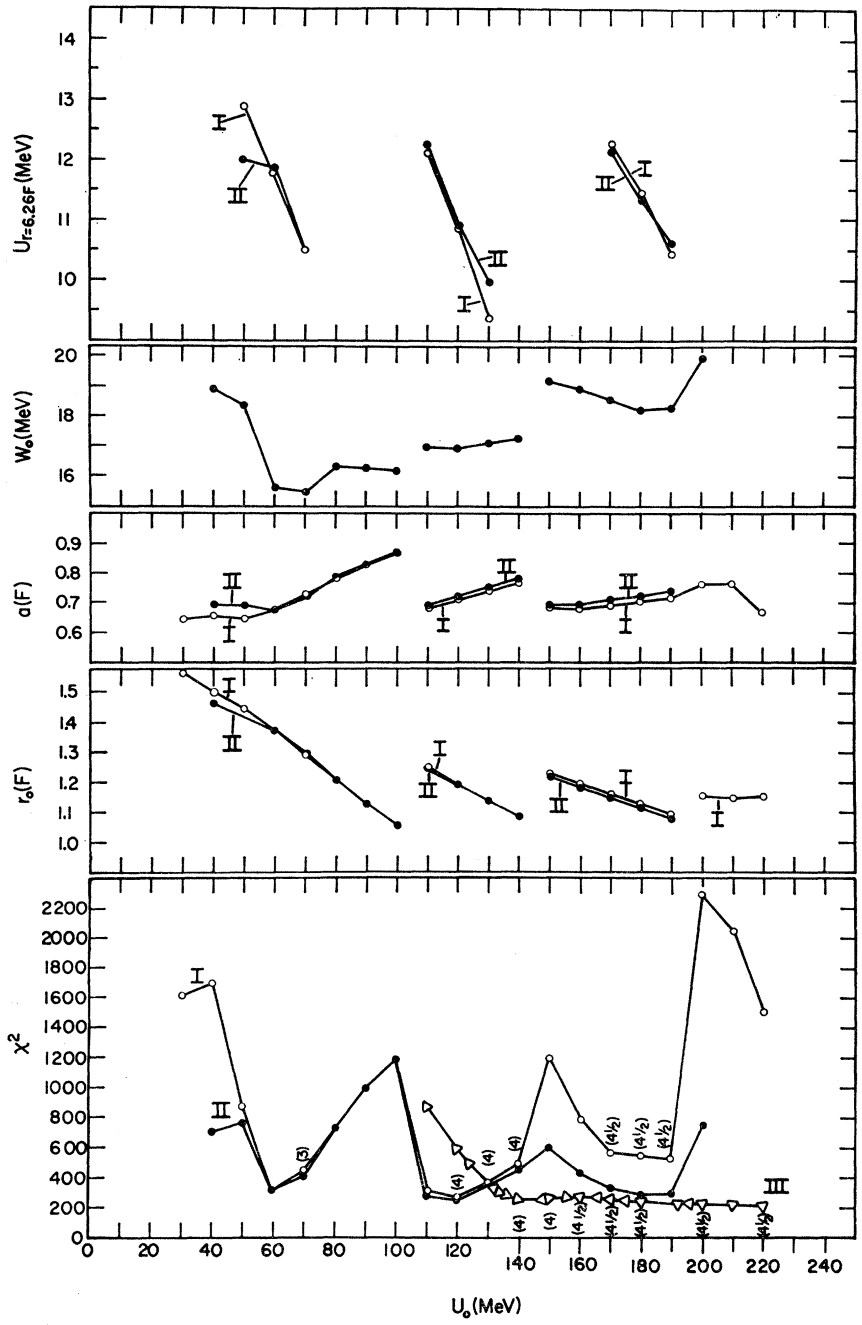

FIG. 4. Variation of the various parameters that resulted from the group-I and -II searches on the 37.7-MeV Ni^{58} data. Plots of χ^2 are also shown as a function of U_0 for group-I, -II, and -III searches. The numbers in parentheses are the number of half-waves for s waves within the nuclear potential. The upper plot shows the value of U at $r=6.26$ F (the radius equal to the classical impact parameter for $L=14$, for which partial wave $|\eta_L|=0.5$).

momenta, as is the case for deuteron and α-particle scattering.[1,2,20] The number of half-wavelengths of s waves for some of the fits is indicated in parentheses on the χ^2 plot in Fig. 4. Partial waves whose first maxima lie in the nuclear surface cannot readjust by an increase in the number of half-waves to preserve the constant values of η_L for the different potentials. For this reason we may anticipate a constraint of parameters that ensures that the potential in the nuclear surface is approximately the same for different discrete ambiguities. That this is indeed so is suggested by the plot in the upper part of Fig. 4 showing the value of U at $r=6.26$ F ($\approx 1.5r_0A^{1/3}$) against U_0. The radius that is chosen here is the classical impact parameter for $L=14$, for which partial wave $|\eta_L|=0.5$.

In the neighborhood of each discrete ambiguity, there is a range of continuous ambiguity where other parameters change in such a way as to compensate changes in U_0. In particular, the product $U_0r_0^n$ is found to remain constant within 2% in such regions. The values of n are 2.38, 1.71, and 1.96 for ambiguities centered on $U_0=60$, 120, and 180 MeV, respectively.

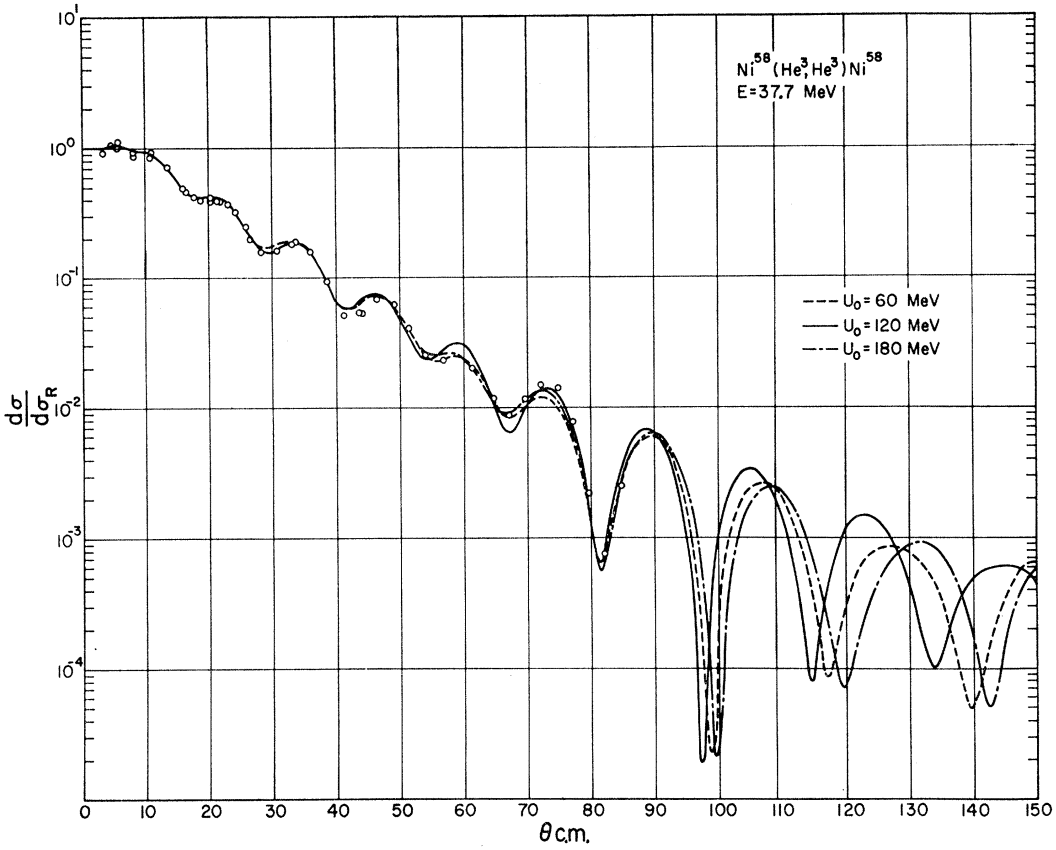

FIG. 5. Comparison of the experimental results with the theoretical angular distributions computed using the optical-model potentials that minimize χ^2 in the group-II search.

Angular distributions predicted by neighboring potentials within the range of a continuous ambiguity are closely similar throughout the complete angular range, and it appears unlikely that more extensive data will succeed in limiting them any further.

The data taken for Zr^{90} at 43.7 MeV cover the widest angular range in these experiments. A group-II search was carried out on this data in the hope of obtaining a more definitive selection of the discrete ambiguities observed for Ni^{58}. Discrete ambiguities were observed for values of U_0 near to 90 MeV ($\chi^2=1686$), 140 MeV ($\chi^2=1364$), and 190 MeV ($\chi^2=1651$). However, the major differences between the predicted angular distributions occurred for angles greater than 130°, again outside the measured angular range. It is interesting that the potentials where the lower two ambiguities occur are different from those for Ni^{58}. This may indicate either that the lower two are unacceptable within the spirit of the optical model, or that the chosen values for the fixed parameters r_0' and a' were not correct.

In the group-III searches on Ni^{58} all five remaining parameters were allowed to vary in minimizing χ^2 for each value of U_0 with the intention of exploring the full extent of the continuous ambiguity centered around $U_0=180$ MeV. A creeping search procedure was adopted to constrain the search to the valley in the χ^2 surface appropriate to this particular discrete ambiguity. In this procedure the starting parameters for a search with a given value of U_0 were the final values that minimized χ^2 in a previous search with a neighboring value of U_0. This process was launched from a parameter set that was close to the one that gave the best fit in group I for $U_0=170$ MeV. The values of χ^2 obtained in this way are compared with those from groups I and II in Fig. 4, and the associated parameter variations are shown in Fig. 6. The χ^2 plot looks like a continuous ambiguity extending from $U_0\approx120$ MeV to the highest assumed value for U_0 at 220 MeV. However, the $l=0$ wave functions were found to change by half a wavelength between $U_0=150$ and 160 MeV. The χ^2 distribution for group III should therefore be interpreted more in the sense of a merging of two discrete ambiguities than stretching of a single one.

In order to proceed with a meaningful systematic analysis of He^3 scattering by different nuclei at various energies, it is necessary to assign fixed values to one member of each pair of parameters whose simultaneous variation would lead to continuous ambiguities. In the analyses described in subsequent sections the geometrical parameters were fixed. Discrete ambiguities

TABLE IV. The standard optical-model parameters. Values of U_0 and W_0 were obtained with a search procedure, while the geometrical parameters were set equal to the standard values described in the text.[a]

Target	E (MeV)	U_0(MeV)	r_0(F)	a(F)	W_0(MeV)	r_0'(F)	a'(F)	χ^2	$\chi^2/(N-F)$
Ca^{40}	37.7	176.9	1.14	0.723	14.5	1.64	0.91	1456	29.71
Fe^{56}	37.7	174.2	1.14	0.723	16.8	1.60	0.81	1267	30.90
Ni^{58}	37.7	172.6	1.14	0.723	16.2	1.60	0.81	600	13.04
Ni^{58}	43.7	171.75	1.14	0.723	17.2	1.60	0.81	2245	45.82
Y^{89}	43.7	175.14	1.14	0.723	14.88	1.60	0.81	4611	107.2
Zr^{90}	43.7	170.0	1.14	0.723	17.42	1.60	0.81	492	6.74

[a] In the heading of the last column, N is the number of data in the angular distribution and F is the number of parameters varied.

that then emerge may be expected to lead to several families of systematic parameters. Not all of these possibilities were followed up and the choice that was made was guided by considerations outlined below.

On the ground of plausibility it has been argued that U_0 for He^3 scattering should be about three times its value for nucleon scattering,[4] i.e., about 150 MeV. For α particles, Wittern estimates a correction resulting from the exclusion principle that will reduce the anticipated potential by some 40 to 70 MeV, depending on bombarding energy. It may be that corrections of a similar order of magnitude will prevail in the case of He^3. Evidence supporting the use of the deeper potentials may be found in processes such as particle-transfer reactions involving He^3 which depend sensitively on the internal wave functions for incoming and outgoing channels. In the $Ca^{40}(He^3,\alpha)$ reaction, Cline *et al.*[7] find that, of three potentials that fit He^3 elastic scattering equally well, only the deepest of these with $U_0\sim180$ MeV will fit the reaction data. Similarly, Drisko and Rybicki[6] are able to fit data from the $Ca^{40}(He^3,p)$ reaction with a He^3 potential of 181 MeV, but not with that of Ref. 10 at 94 MeV. For these reasons, the studies described below were based on parameters associated with the ambiguity with $U_0\sim180$ MeV.

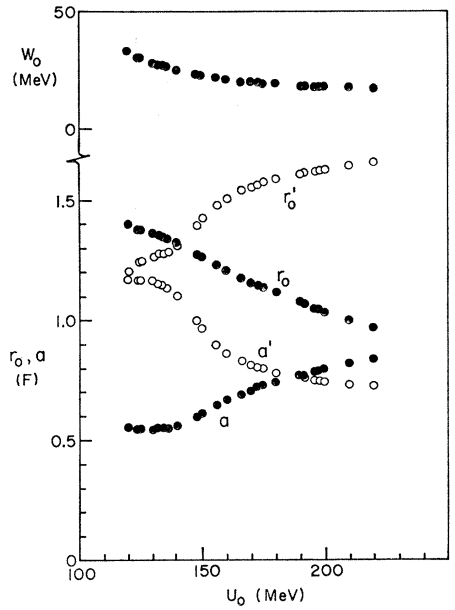

FIG. 6. Variation of the parameters with U_0 that resulted from the group-III search on the 37.7-MeV Ni^{58} data.

VI. DEPENDENCE OF OPTICAL-MODEL PARAMETERS

The possible existence of systematic trends in optical potential well depths as a function of nuclear composition was investigated by analyzing all of the 37.7- and 43.7-MeV data with the same fixed set of geometrical parameters. The standard geometry was arrived at by averaging the geometrical parameters obtained from independent six-parameter searches made to fit data from each of the nuclides. All of these six-parameter searches were started from a set that was related to the ambiguity with the $U_0\approx180$ MeV found for Ni^{58}. Data from each nuclide were then fitted by varying only U_0 and W_0, and the geometrical parameters were assigned the standard values. Values of the parameters so obtained are listed in Table IV. Finally, a second six-parameter search was carried out for each nuclide, starting from parameters that minimized χ^2 for the standard geometry. The "best-fit" parameters thus obtained are shown in Table V.

TABLE V. The optical-model parameters that yielded a minimum value for χ^2 when all parameters were allowed to be varied.[a]

Target	E(MeV)	V_0(MeV)	r_0(F)	a(F)	W_0(MeV)	r_0'(F)	a'(F)	χ^2	$\chi^2/(N-F)$
Ca^{40}	37.7	176.9	1.164	0.654	15.47	1.617	0.975	766	16.65
Fe^{56}	37.7	174.2	1.146	0.689	20.36	1.488	0.928	483	12.71
Ni^{58}	37.7	172.6	1.147	0.712	20.16	1.562	0.802	254	5.90
Ni^{58}	43.7	171.8	1.152	0.703	18.00	1.574	0.918	464	10.09
Y^{89}	43.7	175.2	1.145	0.784	13.96	1.587	0.633	3750	93.75
Zr^{90}	43.7	170.1	1.156	0.689	18.32	1.537	0.876	228	3.25

[a] In the heading of the last column, N is the number of data in the angular distribution and F is the number of parameters varied.

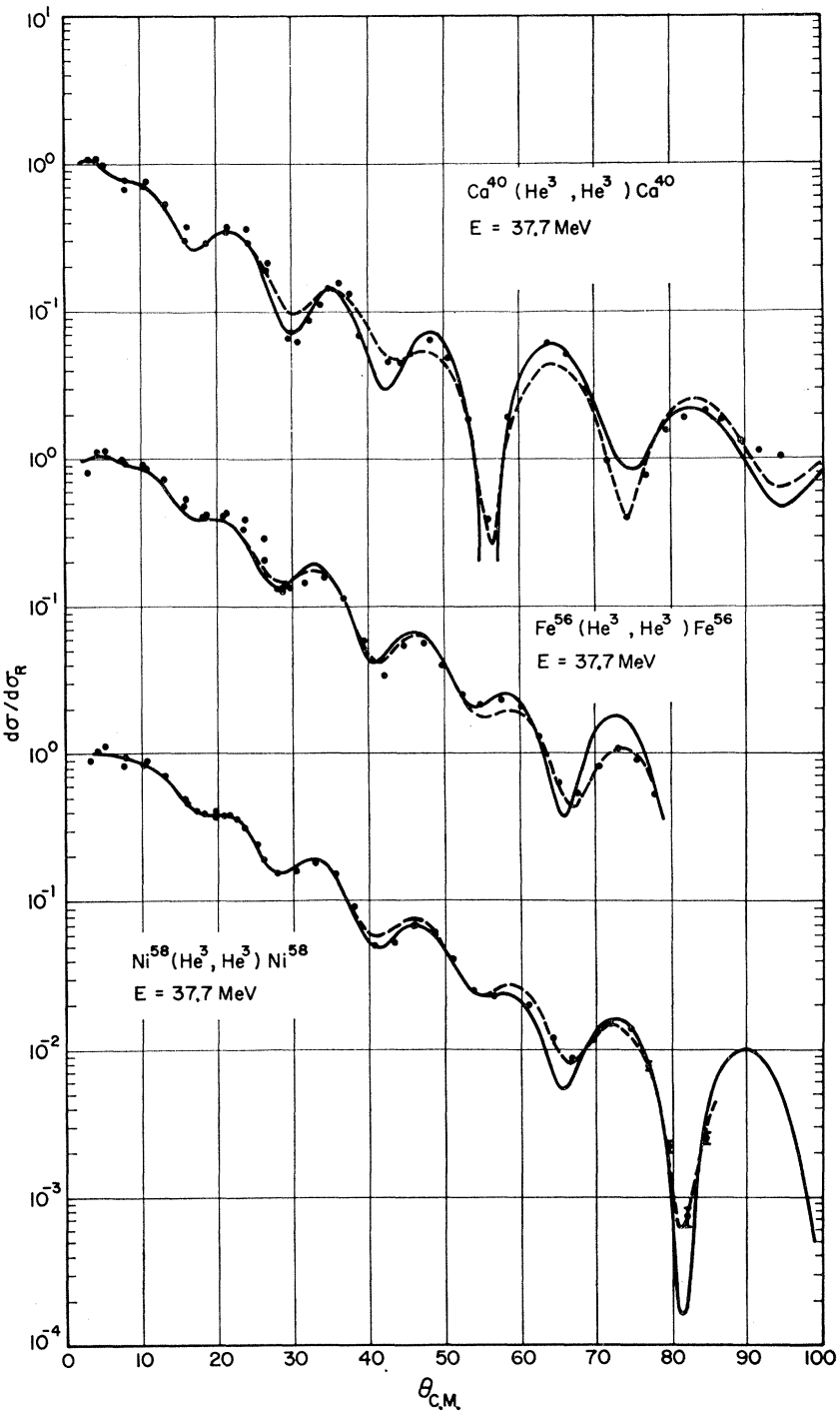

FIG. 7. The elastic angular distributions at 37.7 MeV for Ca^{40}, Fe^{56}, and Ni^{58}. The dashed curves were obtained using optical-model parameters that minimized χ^2 for each nuclide. The solid curves were obtained using the standard geometry discussed in the text.

The quality of fits obtained with the standard geometry are compared in Figs. 7 and 8 with the "best fits" obtained in the second set of six-parameter searches described above. Except in the case of Ca^{40}, the improvement in fit obtained by varying all six parameters is marginal. The fit to Ca^{40} was improved substantially by a small increase in r_0' and a', leaving the geometry of the real well unchanged.

The values of U_0 and W_0 that minimize χ^2 for the standard geometry (r_0' and a' modified for Ca^{40}) are shown in Fig. 9. Values of the parameters as obtained are listed in Table IV. The points for Ca^{40}, Fe^{56}, and Ni^{58} correspond to a bombarding energy of 37.7 MeV and Y^{89} and Zr^{90} to 43.7 MeV. However, the energy dependence of the potentials is so weak for Ca^{40} and Ni^{58} (see Sec. VII) that, if this also applies to Y^{89} and Zr^{90},

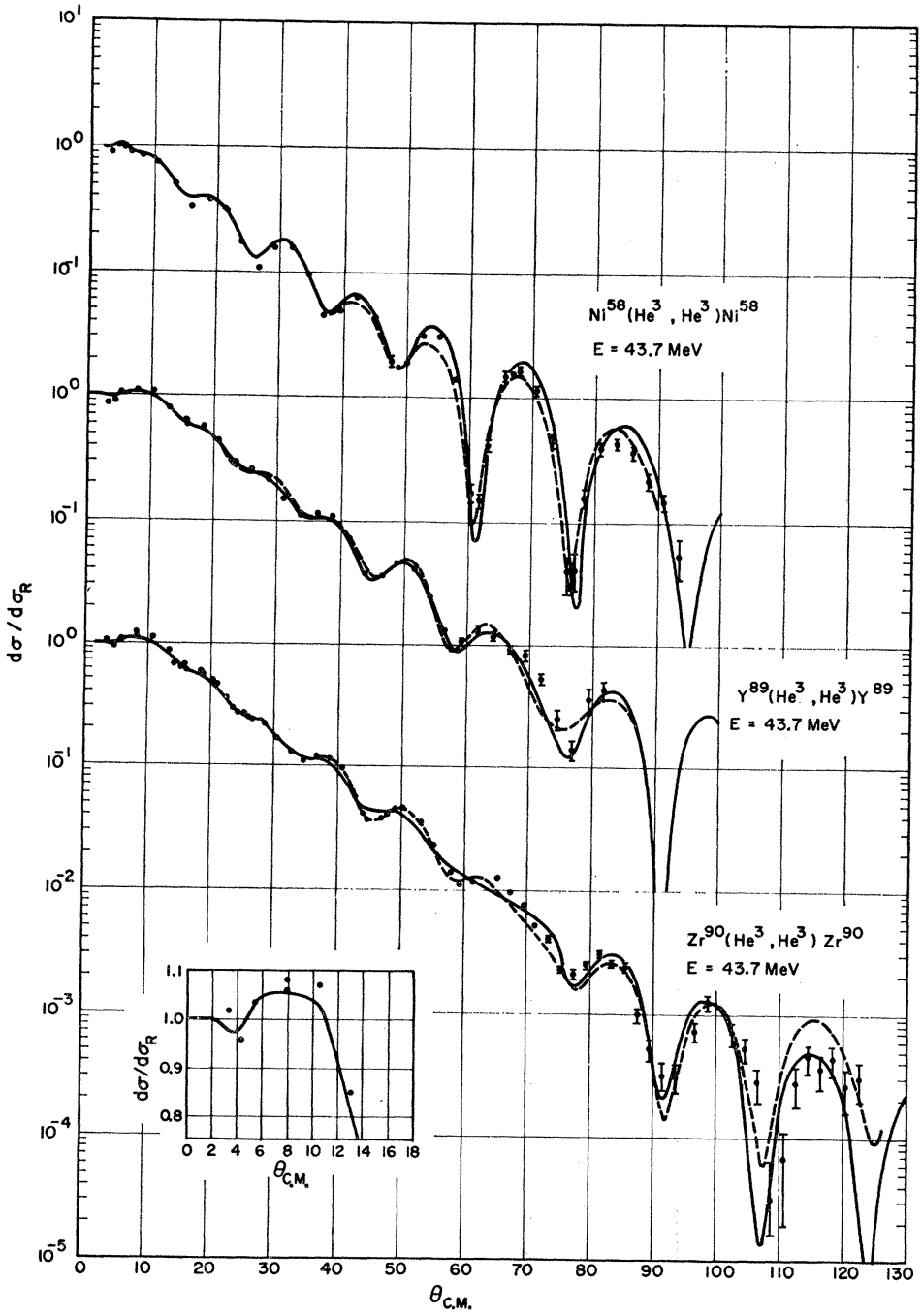

FIG. 8. The elastic angular distributions at 43.7 MeV for Ni^{58}, Y^{89}, and Zr^{90}. The dashed curves were obtained using optical-model parameters that minimized χ^2 for each nuclide. The solid curves were obtained using the standard geometry discussed in the text. The insert is a linear plot of the small-angle Zr^{90} data.

the correction to an energy of 37.7 MeV would be only of the order of 1 MeV for U_0 and W_0, and has been ignored.

The potentials that minimize χ^2 vary very little over the range of A studied in these experiments. No significant reduction in scatter of values of U_0 about their average could be obtained by assuming an isospin dependence of U_0.

VII. ENERGY DEPENDENCE OF THE OPTICAL POTENTIAL

There now exists information on He^3 scattering by Ca^{40} and Ni^{58} over a sufficiently wide range of bombarding energies to justify a study of the possible energy dependence of the optical potentials. In the analysis of energy dependence presented here, use has been made of He^3 scattering data from other laboratories for Ca^{40} at

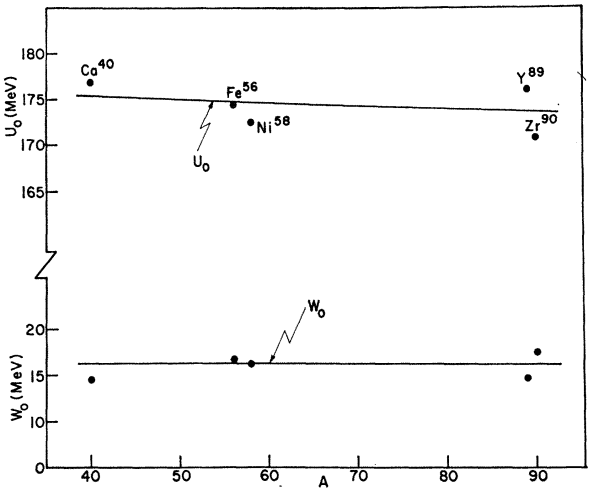

FIG. 9. Values of U_0 and W_0 for the various targets studied that were obtained using the standard optical parameters listed in Table IV.

22 MeV,[12] and 64.3 MeV,[15] and for Ni^{58} at 22 MeV,[12] and 33 MeV,[14] in addition to those from the present experiments for Ca^{40} at 37.7 MeV and Ni^{58} at 37.7 and 43.7 MeV.

In order to minimize uncertainties introduced by continuous parameter ambiguities, the geometrical parameters were again assigned the fixed values given in Table IV for Ca^{40} and Ni^{58}. Two-parameter searches were carried out on each set of data in which only U_0 and W_0 were varied to minimize χ^2. The fits that were obtained for Ca^{40} are shown in Fig. 10, and those for Ni^{58} in Fig. 11. The potentials U_0 and W_0 that gave these fits are plotted against bombarding energy in Fig. 12. The error bar on U_0 for Ni^{58} indicates the uncertainty with which the data determines U_0 under the constraint of fixed geometry.

A systematic energy dependence of U_0, though weak, appears to be demanded by the data, especially for the Ni^{58} target. The variation of W_0 with energy is also

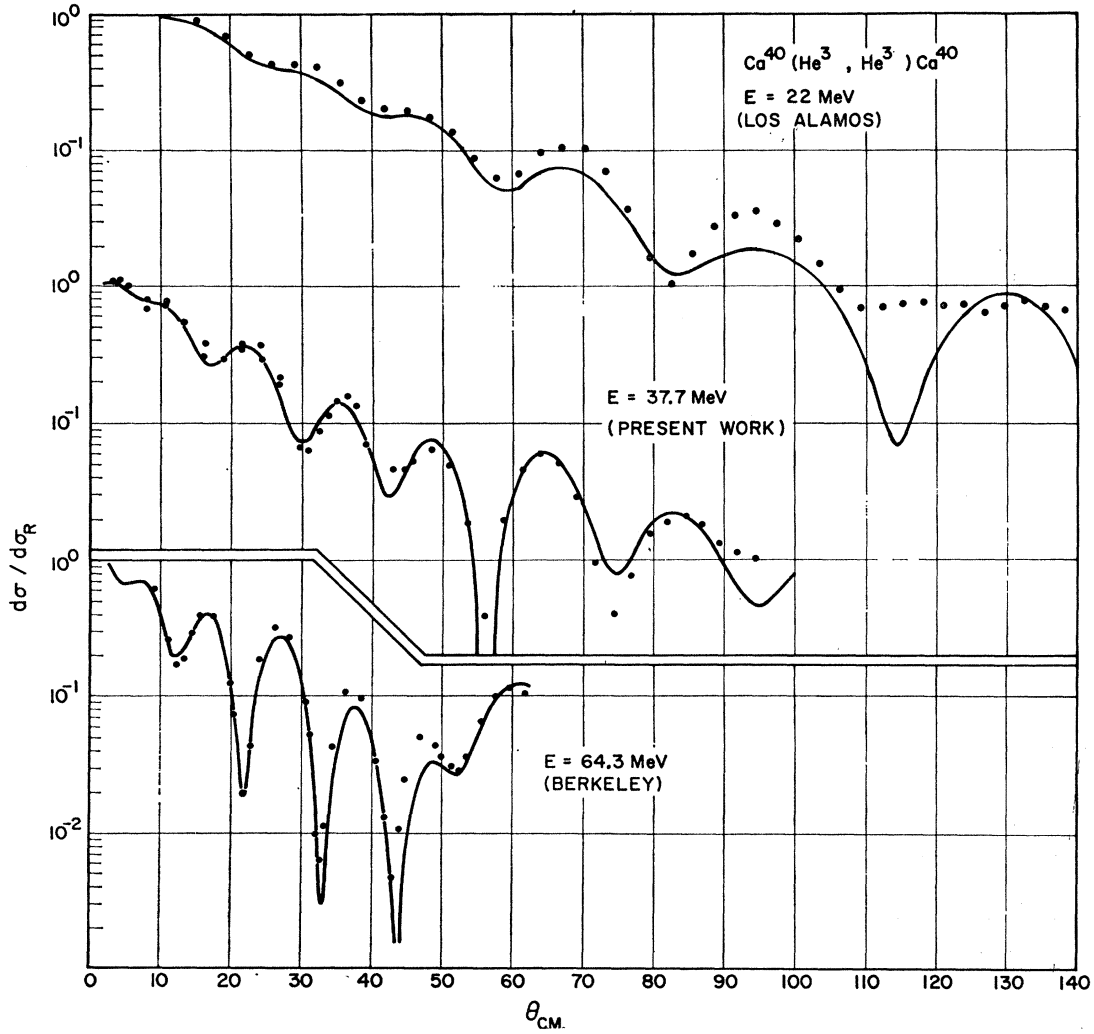

FIG. 10. Elastic angular distributions for Ca^{40} at 22 MeV (Ref. 12), 37.7, and 64.3 MeV (Ref. 15). The solid lines are fits obtained with the geometry given in Table IV for Ca^{40}. The well depths are shown in Fig. 12.

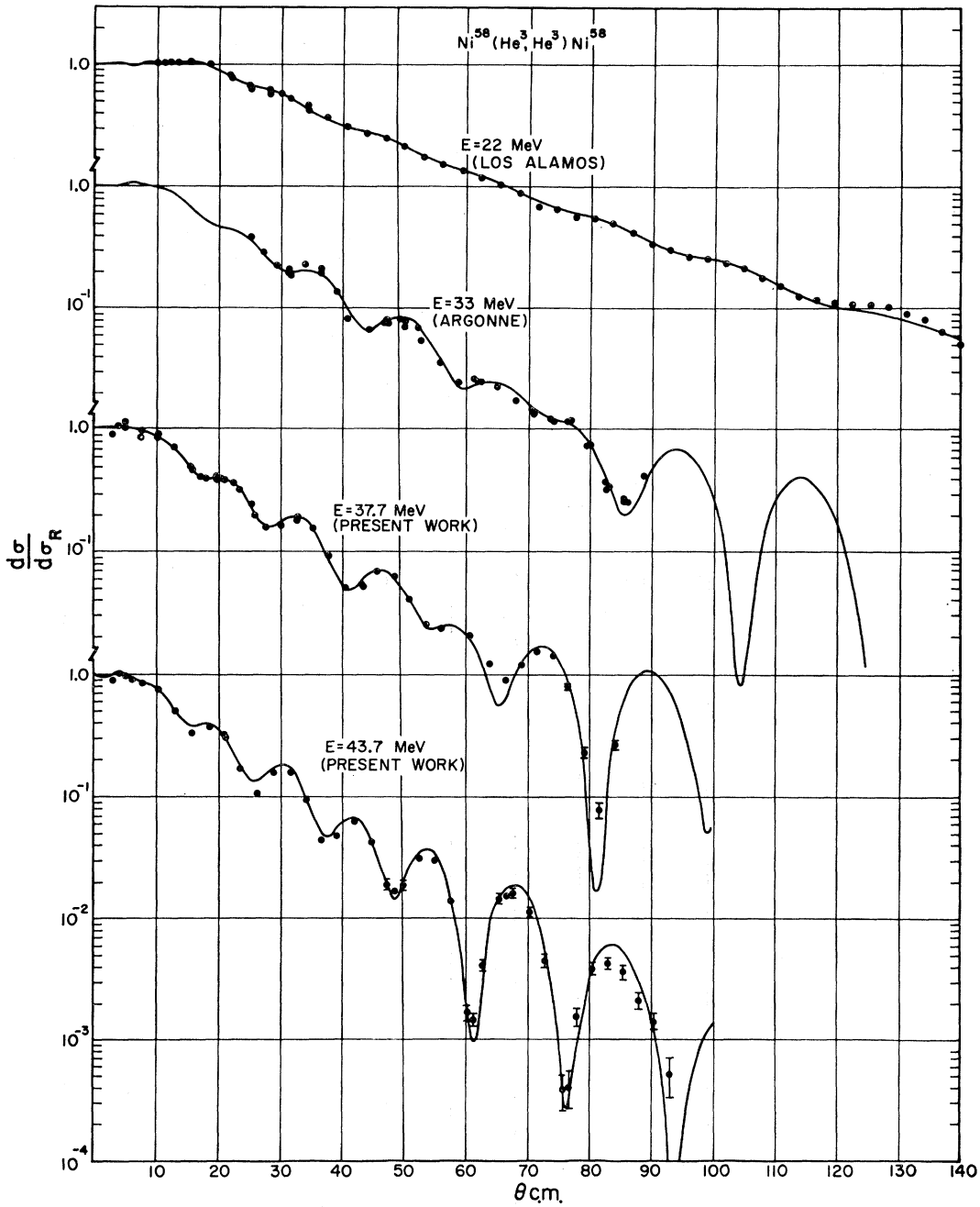

FIG. 11. Elastic angular distributions for Ni^{58} at 22 MeV (Ref. 12), 33 MeV (Ref. 14), 37.7, and 43.7 MeV. The solid lines are fits obtained with the geometry given in Table IV for Ni^{58}. The well depths are shown in Fig. 12.

quite marked for Ni^{58}, and is distinguished from Ca^{40} by a rapid decrease in W_0 with increasing energy for $E<38$ MeV. Both of these effects may merely reflect shortcomings of the optical model. However, it is interesting to conjecture that they reflect the structure aspects of the target. Perey[33] has suggested that the quadrupole excitation is an important source of nonlocality for the optical potential for nucleons. This leads to an increased energy dependence of the real well for vibrations. This excitation is also known to account for a large fraction of the imaginary well depth of the nucleon well.[33] As the energy increases the effect of coupling to this excitation becomes weaker.[33] Presumably such an effect could be important for heavier

[33] F. G. Perey, Phys. Rev. 131, 745 (1963).

projectiles such as the He^3 ion where the effective coupling between the elastic and inelastic channels is stronger. This is currently being checked using coupled channels methods.

VIII. SUMMARY

The optical model has been found to give a good account of the elastic scattering of He^3 ions. Because of the dominance of absorption, many potentials are capable of describing the present data. However, our studies have indicated that additional data at back angles would considerably restrict these ambiguities, particularly those of a discrete nature.

Of the multiple parameter sets which fit the elastic scattering of 37.7-MeV He^3 ions from Ni^{58}, we have selected a set which seems to satisfy the requirements of reaction calculations and which has a real well depth of order three times the potential for nucleons. When applied to the scattering of He^3 ions from other targets and over a wide range of energy, a potential with the same geometry yields acceptable fits with smoothly and slowly varying well depth parameters.

The variation of potentials with mass member does not show any strong dependence on neutron excess such as has been found in the optical potential for nucleons. The parameters may, however, show some dependence on the structure of the target.

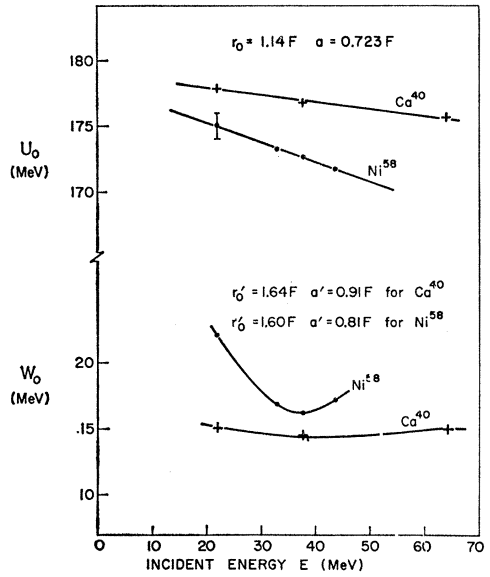

FIG. 12. Real and imaginary well depths as a function of energy for Ca^{40} and Ni^{58}.

ACKNOWLEDGMENTS

We wish to express our appreciation to J. Bane, R. Barnard, and G. Lofgren for help in analyzing the data. We are also indebted to A. G. Blair, M. Chabre, and R. H. Siemssen for use of their elastic-scattering data prior to publication.